Colloids and Surfaces A 589 (2020) 124451

Contents lists available at ScienceDirect

Colloids and Surfaces A

journal homepage: www.elsevier.com/locate/colsurfa

Optical evidence for adsorption of charged inverse micelles in a Stern layer

Bavo Robben[a,*], Filip Beunis[a], Kristiaan Neyts[a], Michiel Callens[b], Thomas Johansson[c], Graham Beales[c], Robert Fleming[b], Filip Strubbe[a]

[a] Electronics and Information Systems Department and Center for Nano and Biophotonics, Ghent University, Technologiepark Zwijnaarde 126, 9052, Zwijnaarde, Belgium
[b] CLEARink Displays, 4020 Clipper Court Fremont, CA 94538 USA
[c] CLEARink Displays, 123 Cambie Street, Suite 600, Vancouver, BC V6B 1B8, Canada

GRAPHICAL ABSTRACT

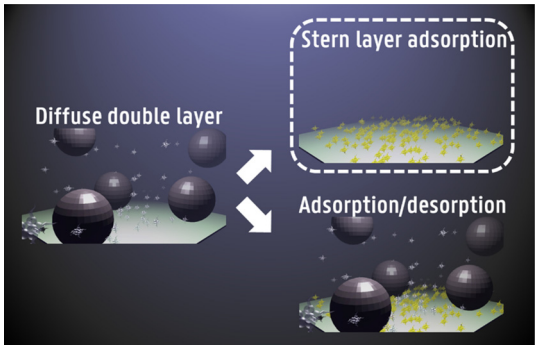

ARTICLE INFO

Keywords:
Inverse micelle
Double-layer capacitance
Nonpolar liquid
Charge adsorption
Stern layer formation

ABSTRACT

Understanding the properties and behavior of nonpolar liquids containing surfactant and colloidal particles is essential for applications such as electrophoretic ink displays and liquid toner printing. Charged inverse micelles, formed from aggregated surfactant molecules, and their effect on the electrophoretic motion of colloidal particles have been investigated in quite some detail over the past years. However, the interactions of charged inverse micelles at the electrode interfaces are still not well understood. In some surfactant systems the charged inverse micelles bounce off the electrodes, while in other systems they are quickly adsorbed to the electrodes upon contact. In this work a fluorocarbon solvent doped with a fluorosurfactant is investigated in which the adsorption of charged inverse micelles to the electrode occurs slowly, leading to long-term charging phenomena. We propose a physical model and an equivalent electrical model based on adsorption and desorption of inverse micelles into a Stern layer with finite thickness. We compare two limiting cases of this model: the 'adsorption/desorption' limit and the 'Stern layer adsorption' limit. Both limits are compatible with electrical measurements. The 'Stern layer adsorption' limit additionally explains the optical measurements, because these measurements indicate that the diffuse double layer vanishes over time when a polarizing voltage step is applied. The obtained value for the Stern layer thickness and the proportionality between the charging time constant and the surfactant concentration are also compatible with the 'Stern layer adsorption' limit.

* Corresponding author.
E-mail address: Bavo.robben@ugent.be (B. Robben).

https://doi.org/10.1016/j.colsurfa.2020.124451
Received 23 October 2019; Received in revised form 8 January 2020; Accepted 9 January 2020
Available online 10 January 2020

1. Introduction

In the last two decades many detailed investigations have been carried out on nonpolar liquids with added surfactant and pigment particles, directed towards applications such as electronic ink displays and liquid toner printing [1–18]. In these dispersions, surfactant acts as a charging agent for colloidal particles, resulting in charged and stabilized colloidal particles [15–18]. At the same time surfactant molecules form inverse micelles of which a small fraction is electrically charged. A few studies have focused on the switching of charged colloidal particles in nonpolar liquids with surfactant [1–5]. In all these studies, complicated electrodynamics are observed because of the effect of electrical charge -from colloidal particles and charged inverse micelles- on the electric field. These studies have made clear that understanding the switching dynamics of colloidal particles requires a more complete understanding of the role of charged inverse micelles. Other studies have focused on the fundamental properties of nonpolar liquids with added surfactant, in the absence of pigment particles, to isolate the effect of charged inverse micelles [6] often based on transient current measurements [7] or impedance spectroscopy measurements [8,9]. For example, the charge stabilization in inverse micelles in nonpolar media has been investigated [10], as well as the equilibrium concentration of charged inverse micelles and its dependency on micelle size and charge generation mechanisms in the bulk and at the interfaces [11]. Various regimes of charge transport have been identified that depend on applied voltage, surfactant concentration and how inverse micelles interact with the electrodes [12]. It has been found that charged inverse micelles of the surfactant OLOA 1200 in dodecane bounce off the electrodes leading to a diffuse double layer of charged inverse micelles at low applied voltages [13]. As a result, transient current measurements of the OLOA 1200system (and equivalently of the very similar OLOA 11,000 system) can be modelled well using a non-sticking boundary condition, leading to a variety of regimes (geometry limited, double-layer limited, space-charge limited, …) [7,12]. In contrast, charged inverse micelles of the well-known surfactant AOT in dodecane stick at the electrodes upon contact when a voltage is applied. Here, an adsorbing boundary condition is appropriate, corresponding to the formation of a Stern layer capacitance [14]. Transient current measurements of the AOT system can be explained using an equivalent electrical network consisting of a bulk conductance and an interface (Stern) capacitance.

Recently, Yezer et al. [9] reported an intermediate situation using the system of Span 80 and Span 20 in dodecane, in which the inverse micelle interaction with the boundary is not simply non-sticking but shows an additional effect on a longer time-scale, related to adsorption of charges from the diffuse double layer at the electrodes. The authors propose a physical model based on adsorption and desorption of charges at the electrodes and an equivalent electrical model that matches well with impedance spectroscopy measurements. They find that the desorption rate constant in their model is proportional to the concentration of surfactant, which cannot be explained by mechanisms with surface species alone but rather requires including another physical desorption mechanism. For example, the authors mention the interaction between surface charges with uncharged bulk micelles.

In this work, we investigate a mixture consisting of a nonpolar fluorosolvent with added fluorosurfactant. We have carried out transient current measurements, which capture essentially the same information as impedance spectroscopy [8,9,19], and find that this system displays a similar behavior as observed by Yezer et al. [9], in which charges from the diffuse double layer are adsorbed at the electrodes. Additionally, measurements are conducted on mixtures with added positively charged pigment particles with a radius between 50 and 200 nm. On these samples total internal reflection measurements are made simultaneously with the transient current measurements. Due to the adsorption of the charged pigment particles the TIR gets frustrated in a region of about 100 nm close to the surface. Such optical measurements provide direct information on the electric field in the region near the electrodes, that is inaccessible by electrical current measurements alone. For example, the optical measurements can reveal whether there is a diffuse double layer or not. More information on this optical measurement method can be found in [1].

The presented study aims to clarify which physical mechanism is at the basis of the observed electrical and optical long-term charging phenomena. We describe a general model which includes adsorption of inverse micelles into a Stern layer with finite thickness and desorption of inverse micelles from the Stern layer. Within this model we compare two limiting cases: the 'adsorption/desorption' limit, equivalent with the model introduced by Yezer et al. [9] where the voltage drop over the Stern layer is neglected and the 'Stern layer adsorption' limit where the desorption of charges is neglected. We assess the agreement of both limits with the observations, by analyzing transient current measurements, total internal reflectivity measurements –where TIR gets frustrated by the adsorption of positively charged pigment particles– and the dependency of the fitting parameters on surfactant concentration measurements from the literature. Both models are equivalent in describing the electrical measurements, and the 'Stern layer adsorption' limit additionally describes total internal reflectivity measurements for polarizing and relaxation voltage steps. Also, the obtained limit for the Stern layer thickness and the proportionality of the time constant with the concentration is in agreement with the 'Stern layer adsorption' limit.

2. Materials and methods

Measurements are carried out on mixtures of surfactant and nonpolar media, with and without colloidal particles. In the first set of measurements, (charged) inverse micelles are obtained by mixing surfactant molecules with a low dielectric constant solvent. This mixture consists of a fluorocarbon surfactant in a nonpolar fluorosolvent (dielectric constant ε about 7) without absorbing particles, with surfactant concentration far above the critical micelle concentration. The mixture is inserted into a measurement device consisting of two parallel, ITO-coated glass (n = 1.51, 15 Ω/sq) substrates, that are kept at a distance d of 15 μm using spherical glass spacers. The overlapping area S of the patterned ITO electrodes is 1 cm^2. The glass substrates are glued together with UV curing glue (Norland, NOA 68).

Transient current measurements are performed with a Keithley 428 current amplifier. Initially the two ITO electrodes are short-circuited for at least 100 s. Then, a polarizing voltage with amplitude V_A = 0.05 V is applied for a polarizing time t_p ranging between 1 and 200 s. After this, the voltage amplitude is reduced to $V_A/2$ for a duration of 50 s. Finally, the voltage is set to zero for at least one hundred seconds to restore a homogenous state. This sequence is repeated for different polarizing times t_p. The device under test is shielded from external electrical interference to obtain picoampere resolution. Data acquisition is achieved with a NI DAQ device (NI USB-6212 BNC).

A second set of measurements is again based on a mixture consisting of the same fluorosurfactant, with surfactant concentration far above the critical micelle concentration, in a nonpolar fluorocarbon solvent (with dielectric constant ε about 4 and refractive index $n \approx 1.3$) and a few volume percent pigment particles with radius between 50 and 200 nm. The mixture is inserted in a similar measurement device consisting of two parallel, ITO-coated glass substrates. For this second set of experiments, to avoid that pigment particles chemically bind with the interface, the ITO surfaces are silane-treated. Any influence of this monolayer on the interface capacitance is included in the Stern layer capacitance.

Transient current measurements (as explained above) and total internal reflectivity (TIR) measurements are performed simultaneously. The reflectivity under total internal reflection at the ITO/liquid interface is determined by measuring the intensity of a reflected laser beam (continuous CrystaLaser, 532 nm) which is coupled into the glass

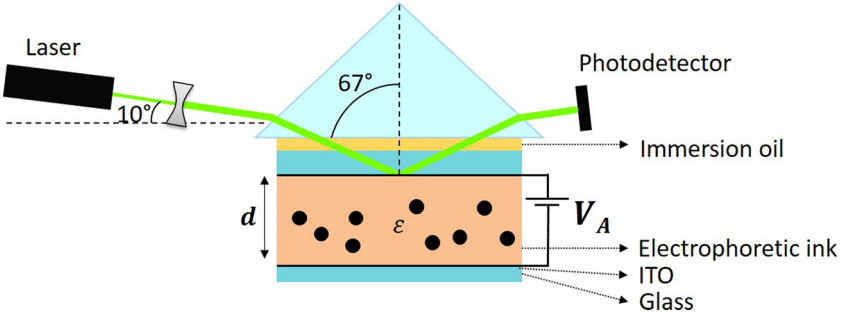

Fig. 1. Schematic of the setup for the total internal reflection measurement of an electrophoretic device, when a potential difference V_A is applied. The incident laser beam (532 nm) makes an angle of 10° with the horizontal and is attenuated and expanded to 5 mW and 1 mm diameter. A 45° prism is in optical contact with the top glass substrate by immersion oil, allowing incidence at 67°, above the critical angle of 59° needed for TIR. The intensity of the reflected beam is measured with a photodetector.

substrate at a large angle of incidence using a 45° prism, as shown in Fig. 1. Due to the adsorption of pigment particles we have frustration of the TIR resulting in a decrease of the reflectivity. The optically probed side is at the electrically grounded side. Prior to each measurement, the two ITO electrodes are short-circuited for at least 100 s. Then, a polarizing voltage with amplitude V_A is applied for 3000 s. Next, the device is relaxed by applying 0 V for 3000 s. Then, a negative polarizing voltage with amplitude V_A is applied for 3000 s. Finally, the cell is relaxed again (0 V). This sequence is performed for $V_A = 0.1$ V and $V_A = 0.2$ V.

More information on the combined transient current measurements with TIR can be found in [1].

Note that the solvents used in both sets of experiments have a different dielectric constant. For the second set, the particle mixture is as provided by Merck. For the first set of measurements we choose a nonpolar fluorosolvent with a higher dielectric constant. Due to the higher dielectric constant a larger fraction of the inverse micelles is charged resulting in thinner diffuse double layers, a higher charge concentration in the diffuse double layer near the interface, and a reduced Stern layer time constant according to Eqs. (5) and (8) as explained further below. This smaller τ_{eff} leads to shorter and more practical measurements.

3. Measurement results

Next, we show the results from two sets of experiments. Firstly, transient currents are measured for the solvent-surfactant mixture (in the absence of pigment particles). Here, a nonpolar solvent with a relatively high dielectric constant is chosen, which has the practical advantage that the transient phenomena of interest occur in a relative short time. A particular driving scheme, namely a switch of 0 to V_A and back to $V_A/2$, is chosen because this clearly illustrates the effect of the duration of the polarizing pulse on the long-term current at $V_A/2$. Secondly, we show measurements of the mixture with positively charged pigment particles. On this system, besides transient current measurements also TIR measurements are carried out which are based on light-absorption by pigment particles in the evanescent field region. These measurements provide insight in the electric field close to the electrode-liquid interface, which is crucial for determining the dominant charging mechanism at this interface.

Fig. 2 shows the transient current measurements for fluorosurfactant in fluorocarbon solvent, after switching on (from 0 V to $V_A = 0.05$ V) and after reducing the voltage by a factor two (from 0.05 V to 0.025 V at t_p), for $t_p = 1$ s (blue), 2 s, … 200 s (red). Fig. 2a shows the current up to 1 s, Fig. 2b shows the current between 0.1 s and 100 s in more detail.

For the polarizing voltage step (from 0 V to 0.05 V) the initial current I_0 is 54 nA/cm^2 and over the time range $10^{-4} - 10^{-1}$ s the current decays approximately exponentially with a time constant $\tau_{DL} = 40$ ms (see Fig. 2a). Around 1 s a current level I_{s0} of about 1.8nA/cm^2 is observed, after which the current further decreases exponentially with a time constant τ_s of 52 s (see Fig. 2b). The polarizing current is similar for all values of t_p, which confirms that the relaxation time of 100 s between consecutive measurements is long enough to restore a homogeneous state.

After the voltage is reduced by a factor two (from 0.05 V to 0.025 V) the current starts at $I_0 = -26$nA/cm^2 and the amplitude decreases exponentially over the time range $10^{-4} - 10^{-1}$ s with the same time constant $\tau_{DL} = 40$ ms as for the polarizing current (see Fig. 2a). At $t = 1$ s a current $I_{s0,d}$ is observed which is strongly dependent on the duration t_p of the polarizing voltage step (see Fig. 2b). Fig. 2c shows the current $I_{s0,d}$ versus the polarizing time t_p. When the duration of the polarizing pulse is short compared to the long-term exponential decay ($t_p \ll \tau_s$) we find $I_{s0,d} = 0.87$nA/cm$^2 \approx \frac{I_{s0}}{2}$. When the duration of the polarizing pulse is long compared to the long-term exponential decay ($t_p > \tau_s$) we find $I_{s0,d} = -0.75$nA/cm$^2 \approx -\frac{I_{s0}}{2}$. These currents decrease exponentially with about the same time constant $\tau_s = 52$ s.

The second set of measurements is based on a similar mixture of surfactant in a low dielectric solvent, but now with the addition of pigment particles (see Materials and methods). The transient current and the reflectivity by TIR are measured simultaneously. The electric current measurement is shown in Fig. 3a. The total internal reflectivity (normalized by setting the value without particles equal to one) is shown in Fig. 3b. Polarizing measurements for a voltage step from 0 V to $V_A = 0.1$ V and 0.2 V are visualized in red. Relaxation measurements (switching back to 0 V) after a polarizing step of $V_A = -0.1$ V and -0.2 V with a duration $t_p = 3000$ s are visualized in green. The polarizing measurements with amplitude V_A (red) match well with the relaxation measurements after a 3000 s polarizing step with the same amplitude V_A but with opposite polarity (green).

The transient currents for $t < 1$ s are exponentially decreasing (not shown in Fig. 3a), similarly as in Fig. 2a. Around 10 s the measurements show a current of 1.55 nA/cm^2 and 3.1nA/cm^2 for 0.1 V and 0.2 V, respectively, after which the current further decreases exponentially with a decay time constant $\tau_s = 450$ s.

The TIR measurements in Fig. 3b show a high initial reflectivity which decreases and reaches a minimum around 35 s. The minimal reflectivity is 0.8 and 0.4 for 0.1 V and 0.2 V, respectively. Between 100 s and 1000 s, the reflectivity slowly increases again and returns to the initial value.

4. Charge transport model

In this section we introduce a model for the transport of inverse micelles. We first briefly introduce the double layer limited regime to explain the short time behavior (more information can be found in [12]). Afterwards, we develop a theoretical model for the long term behavior with the aim of explaining the experimental results of the previous section.

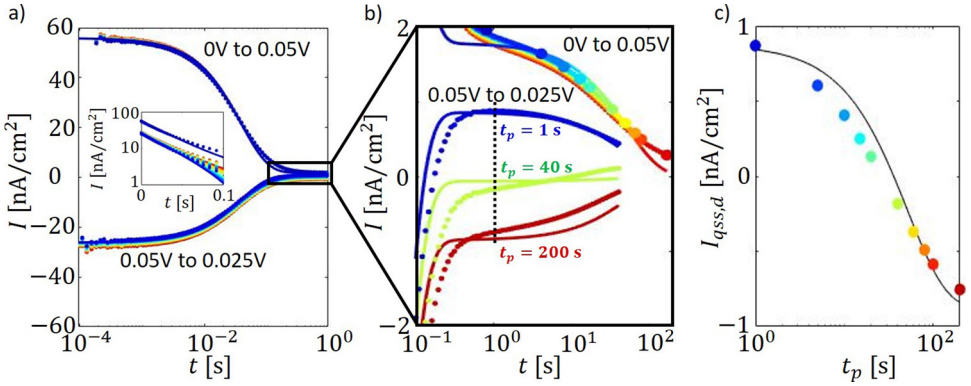

Fig. 2. Electrical current measurement after switching from 0 to V_A (with duration t_p = 1 s (blue), 5 s, …, up to 200 s (red)); and current after switching from V_A to $\frac{V_A}{2}$ with duration 50 s. a) Visualization of the short time for $t < 1$ s. The inset visualizes the absolute values of the current on a semi-log plot b) Visualization at low current levels with a long time range 0.1 s< t < 200 s. c) Visualization of the amplitude of the current at 1 s after the voltage was reduced versus the duration of the polarizing time t_p. Full lines represent the theoretical result based on the 'Stern layer adsorption' limit (Eq. (16)) with G_b = 1.08μS/cm^2, λ_{DL} = 69 nm, G_s = 71 × 10^{-9} S/cm^2 and d_s = 1.6 nm.

For the behavior during the polarizing pulse for $t < 0.1$ s in Fig. 2a we can rely on the well-established theory of diffuse double layer charging. In this theory, positively and negatively charged inverse micelles are considered with equal electrophoretic mobility μ, diffusion coefficient D and initial concentration $\bar{n}$. The transport of charged inverse micelles is governed by drift and diffusion, and inter-particle interactions are ignored. It is assumed that these charged inverse micelles do not stick to the surface of the electrodes. When the charge content is high and the applied voltage low, as is the case here ($\lambda = \frac{2e}{\varepsilon\varepsilon_0 V_T}\bar{n}d^2 > 100$ and $V_A \cong \frac{2k_bT}{e}$, with λ the dimensionless charge content defined in [12], ε_0 the dielectric constant of the solvent, ε the vacuum permittivity, V_T the thermal voltage, k_b the Boltzmann constant, T the temperature and e the elementary charge) [12], the theory predicts screening of the electric field in the bulk due to buildup of charge in the diffuse double layers. When a voltage is applied, the initial current per unit surface area is given by $I_0 = 2e\mu\bar{n}V_A/d$. The characteristic time constant for exponential decay is [12]:

$$\tau_{DL} = \frac{\varepsilon\varepsilon_0 d}{4e\mu\bar{n}\lambda_{DL}} \tag{1}$$

with $\lambda_{DL} = \sqrt{\frac{\varepsilon\varepsilon_0 k_b T}{2e^2\bar{n}}}$ the Debye length and the diffuse double layer thickness. This behavior can be modelled by an equivalent electrical circuit consisting of a conductor with conductance G_b per unit surface area representing the bulk conductivity of the device in series with two capacitors with capacitance C_{DL} per unit surface area representing the diffuse double layers at the two electrodes:

$$G_b = \frac{2e\bar{n}\mu}{d} \tag{2}$$

$$C_{DL} = \frac{\varepsilon\varepsilon_0}{\lambda_{DL}} \tag{3}$$

with $\tau_{DL} = \frac{1}{G_b}\frac{C_{DL}}{2}$. The current per unit surface area for $t < 0.1$ s can therefore be approximated by [12]:

$$I_{DL}(t) = I_0 \exp\left(-\frac{t}{\tau_{DL}}\right) \tag{4}$$

The observation in Figs. 2b and 3 a of a persisting current between 0.1 s and 1000 s indicates that there is an additional transport mechanism. Firstly, we propose, just like in the case of AOT micelles in dodecane [14], that charged inverse micelles present in the diffuse double layer are getting adsorbed at the electrode surface. At the electrode they form a Stern layer in which the charge of the inverse micelles remains at a distance d_s, equal to half of the inverse micelle radius, from the electrode. Secondly, we consider that charges can desorb from the Stern layer by introducing a desorption rate τ_d. We first will elaborate the solution of the linearized differential equation before providing an equivalent circuit model. Note that all formulas are derived for the optically probed side which is electrically grounded; the formulas for the opposite side (where the voltage is applied) can be found similarly.

We assume that the increase of the Stern layer surface charge density π_s per unit time, $k_a\rho_{DL,s}$, is due to adsorption of inverse micelles in the Stern layer, which is proportional to the net charge density $\rho_{DL,s}$ in the diffuse double layer closest to the interface, with k_a the adsorption rate constant in m/s. The charge in the Stern layer decreases over time due to desorption of the charges present in the Stern layer with a desorption time constant τ_d resulting in a decrease of the Stern layer charge density per unit time with $-\frac{\pi_s}{\tau_d}$. The combination of adsorption and desorption results in:

$$\frac{d\pi_s}{dt} = k_a\rho_{DL,s} - \frac{\pi_s}{\tau_d} \tag{5}$$

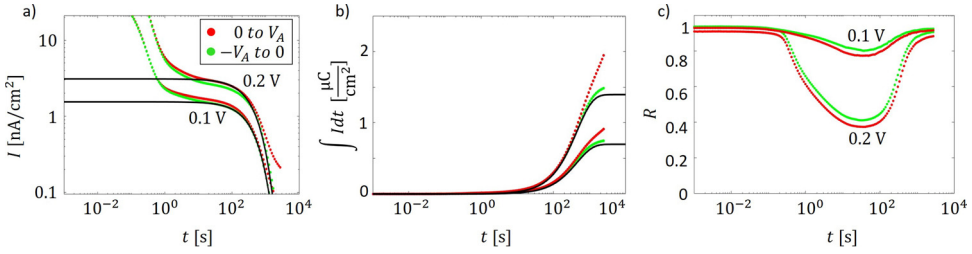

Fig. 3. a) Current measurement b) Integrated current and c) reflectivity measurement for a fluorocarbon based black ink, for voltage steps from 0 to V_A (polarizing, red) and $-V_A$ to 0 (relaxation after a 3000 s negative polarizing step, green) with amplitude 0.1 V and 0.2 V. In a) and b) Exponential fits are provided in black with amplitude 1.55 nA/cm^2 and 3.1 nA/cm^2 for 0.1 V and 0.2 V, respectively. Both have a time constant of 450 s. (For interpretation of the references to colour in this figure legend, the reader is referred to the web version of this article).

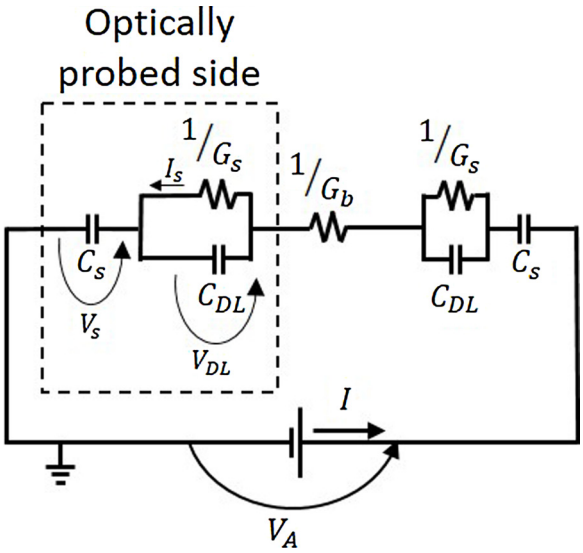

Fig. 4. Equivalent electrical circuit of the 'Stern layer adsorption' limit, with bulk conductance G_b, diffuse double layer capacitance C_{DL}, Stern layer formation conductance G_s and Stern layer capacitance C_s. The electrode resistance R_e and the cell capacitance C_g are not shown because $R_e C_g \ll \frac{1}{G_b} C_{DL}$.

According to the diffuse double layer theory we find that the net charge density close to the surface is proportional to the voltage drop V_{DL} over the diffuse double layer: $\rho_{DL,s} = \frac{\varepsilon\varepsilon_0}{\lambda_{DL}^2} V_{DL}$ [12]. Based on the capacitive nature of the Stern layer we also find that $V_s = \pi_s \frac{d_s}{\varepsilon\varepsilon_0}$. After the diffuse double layers are established ($t \gg \tau_{DL}$) we assume that the sum of the voltage drop over the diffuse double layers and Stern layers is equal to the applied voltage, meaning that the bulk field is completely screened: $\frac{V_A}{2} = V_s + V_{DL}$. Based on these relations we can rewrite Eq. (5):

$$\frac{d\pi_s}{dt} = k_a \frac{\varepsilon\varepsilon_0}{\lambda_{DL}^2}\left(\frac{V_A}{2} - \pi_s \frac{d_s}{\varepsilon\varepsilon_0}\right) - \frac{\pi_s}{\tau_d} \tag{6}$$

If we combine the factors proportional to the surface charge density, we can rewrite this in a simplified linear differential equation of first order:

$$\frac{d\pi_s}{dt} = -\frac{\pi_s}{\tau_{eff}} + \frac{k_a \varepsilon\varepsilon_0}{\lambda_{DL}^2}\frac{V_A}{2} \tag{7}$$

$$\frac{1}{\tau_{eff}} = k_a \frac{d_s}{\lambda_{DL}^2} + \frac{1}{\tau_d} \tag{8}$$

with an effective time constant τ_{eff}. Solving Eq. (7) for the surface charge density results in:

$$\pi_s = \frac{k_a \varepsilon\varepsilon_0}{\lambda_{DL}^2}\frac{V_A}{2}\tau_{eff}\left(1 - \exp\left(-\frac{t}{\tau_{eff}}\right)\right) \tag{9}$$

Since the surface charge density changes over time, the voltage drop over the Stern layer changes over time resulting in a change in the voltage drop over the diffuse double layer. This implies that Q_{DL}, the charge in the diffuse double layer per unit surface area, changes over time as:

$$Q_{DL} = V_{DL} C_{DL} = \frac{V_A}{2}\frac{\varepsilon\varepsilon_0}{\lambda_{DL}} - \frac{d_s}{\lambda_{DL}}\frac{k_a \varepsilon\varepsilon_0}{\lambda_{DL}^2}\frac{V_A}{2}\tau_{eff}\left(1 - \exp\left(-\frac{t}{\tau_{eff}}\right)\right) \tag{10}$$

For $d \gg \lambda_{DL}$ the external current per unit surface area $I(t)$ for $t > \tau_{DL}$ can be approximated by the charge accumulation in the Stern layer $d\pi_s/dt$ found by plugging Eq. (9) into Eq. (7):

$$I(t) = \frac{k_a \varepsilon\varepsilon_0}{\lambda_{DL}^2}\frac{V_A}{2}\left(\exp\left(-\frac{t}{\tau_{eff}}\right)\right), \quad t > \tau_{DL} \tag{11}$$

Therefore, according to the present theory the external current in Eq. (11) follows an exponential decay with fitting parameters k_a and τ_{eff}. Knowing τ_{eff}, one can introduce a lower boundary for τ_d and an upper boundary for d_s based on Eq. (8):

$$\begin{cases} \tau_d \geq \tau_{eff} \\ d_s \leq \dfrac{\lambda_{DL}^2}{k_a \tau_{eff}} \end{cases} \tag{12}$$

We can consider two limiting cases: the 'adsorption/desorption' limit, in which we neglect the voltage drop over the Stern layer by setting the Stern layer thickness zero ($\tau_d = \tau_{eff}$, $d_s = 0$), and the 'Stern layer adsorption' limit, in which we neglect the charge desorption ($\tau_d = \infty$, $d_s = \frac{\lambda_{DL}^2}{k_a \tau_{eff}}$). An important difference between these two limits emerges in the amount of charge which is present in the diffuse double layer calculated with Eq. (10):

$$Q_{DL}(t) = \begin{cases} \dfrac{V_A}{2}\dfrac{\varepsilon\varepsilon_0}{\lambda_{DL}} \text{ ('adsorption/desorption' limit)} \\ \dfrac{V_A}{2}\dfrac{\varepsilon\varepsilon_0}{\lambda_{DL}} \exp\left(-\dfrac{t}{\tau_{eff}}\right) \text{ ('Stern layer adsorption' limit)} \end{cases} \tag{13}$$

The former 'adsorption/desorption' limit, is carefully elaborated by Yezer et al. [9] where also an equivalent electrical network is proposed which makes the understandings more intuitive. In the following, we will explore the latter, namely the 'Stern layer adsorption' limit. Further below, in the discussion section we will then show that the 'adsorption/desorption' limit is also able to explain the optical measurements.

In order to describe the equivalent electrical network for the 'Stern layer adsorption' limit we can describe the proportionality between the charge adsorption k_a and the voltage drop over the diffuse double layer V_{DL} using a Stern layer formation conductance per unit surface area:

$$G_s = \frac{k_a \varepsilon\varepsilon_0}{\lambda_{DL}^2} \tag{14}$$

The adsorption of charges at a distance d_s from the electrode results in a capacitive voltage drop represented by the Stern layer capacitance per unit surface area:

$$C_s = \frac{\varepsilon\varepsilon_0}{d_s} \tag{15}$$

The related RC or C/G time constant is $\tau_{eff} = \frac{\lambda_{DL}^2}{k_a d_s}$.

Based on the equivalent electrical circuit elements given by Eqs. (2) (3)(14) and (15) the equivalent electrical circuit model is shown in Fig. 4. In the limit of slow Stern layer adsorption (i.e. assuming $\frac{1}{G_s} \gg \frac{1}{G_b}$ and $\frac{1}{G_s} C_s \gg \frac{1}{G_b} C_{DL}$), the electrical model can be simplified, and the slow and fast RC characteristics can be decoupled as follows: For the short-term behavior, we obtain RC characteristics due to G_b (representing the bulk liquid conductance given by Eq. (2)) and C_{DL} (representing the diffuse double layer capacitance given by Eq. (3)). For the long-term behavior, we find RC characteristics due to G_s (representing adsorption of charges from the diffuse double layer into the Stern layer given by Eq. (14)) and C_s (representing the Stern layer capacitance given by Eq. (15)). The electrode resistance R_e and the cell capacitance C_g are not shown because $R_e C_g \ll \frac{1}{G_b} C_{DL}$. This decoupled equivalent electrical network can be solved analytically:

$$I(t) = I_0 \exp\left(-\frac{t}{\tau_{DL}}\right) + I_s(t) \tag{16}$$

$$I_s(t) = G_s V_{DL}(t) \tag{17}$$

$$V_{DL}(t) = \frac{V_A}{2} - \frac{\pi_s(t)}{\varepsilon\varepsilon_0} d_s \tag{18}$$

$$\frac{d}{dt}\pi_s(t) = I_s(t) \tag{19}$$

In Eq. (16), $I_0\exp\left(-\frac{t}{\tau_{DL}}\right)$ is the current per unit surface area related to the formation of the diffuse double layers at both electrodes and $I_s(t)$ is the current per unit surface area related to the diffuse double layer to Stern layer transition. In Eq. (17), $V_{DL}(t)$ is the voltage drop over the diffuse double layer, d_s is the charge-electrode distance for the adsorbed charges in the Stern layer. In Eq. (18) $\pi_s(t)$ is the Stern layer surface charge density. Eqs. (16)–(19) can be solved for a step function of the applied voltage at $t = 0$ s, where $\pi_s(0)$ represents the Stern layer charge density at $t = 0$, to obtain the Stern layer formation current per unit surface area:

$$I_s(t) = G_s\left(\frac{V_A}{2} + \frac{\pi_s(0)d_s}{\varepsilon\varepsilon_0}\right)\exp\left(-\frac{t}{\tau_s}\right) = \frac{C_s V_A/2 + \pi_s(0)}{\tau_s} exp(-\frac{t}{\tau_s}) \quad (20)$$

Here, $\tau_s = \frac{C_s}{G_s}$ is the Stern layer exponential decay time. The initial surface charge density $\pi_s(0)$ is equal to 0 for the polarizing voltage step. The initial surface charge density $\pi_s(0)$ for the transition from V_A to $V_A/2$ is equal to the charge density which has been accumulated in the Stern layer during the preceding polarizing step: $\frac{C_s V_A}{2\tau_s}\left(1 - \exp\left(-\frac{t_p}{\tau_s}\right)\right)$.

The results of the theoretical model (Eqs. (16)–(20)) are plotted as full colored lines in Fig. 2, with parameters chosen to match the experimental results: $I_0 = 54\text{nA/cm}^2$, $\tau_{DL} = 40$ ms, $G_s = 71\,\text{nS/cm}^2$ and $\tau_s = 51$ s, resulting in $G_b = 1.08\,\mu\text{S/cm}^2$, $C_{DL} = 86\,\text{nF/cm}^2$ and $d_s = 1.6$ nm. Based on the diffuse double layer theory (Eqs. (1)–(4)) we can relate these circuit model parameters with physical parameters of the inverse micelle system: $\lambda_{DL} = 69$ nm, $\bar{n} = 9.8 \times 10^{20}\,\text{m}^{-3}$ and $\mu = 0.5 \times 10^{-9}\text{m}^2/\text{Vs}$.

Note that this model assumes that the concentration of charged inverse micelles in the bulk does not change. A closer look at the amount of charge needed to build up the Stern layer shows that the collected charge in the Stern layer is of the same order of magnitude as the total initial charge in bulk. However, since the diffuse double layer to Stern layer process is slow compared to the disproportionation/comproportionation process in the bulk [20] and the concentration of neutral micelles is much larger than the concentration of charged micelles, we expect this assumption to be valid. The fact that the initial currents, after reducing the voltage to $\frac{V_A}{2}$, overlap for all τ_p supports the assumption that the bulk charge doesn't change during accumulation. We can neglect leakage currents supported by the fact that we don't measure dominant resistive losses in the system (the integrated current in the polarizing step is approximately equal to the integrated current during relaxation, visualized in Fig. 3b).

5. Discussion

Let us now analyze in more detail the electrical current measurements of Fig. 2 using the above described 'Stern layer adsorption' limit model, assuming the desorption of charges from the Stern layer is negligible. We examine what happens if the applied voltage is reduced from V_A to $\frac{V_A}{2}$ at a time t_p when the Stern layer has been charged to a value $\pi_s = \frac{C_s V_A}{2\tau_s}\left(1 - \exp\left(-\frac{t_p}{\tau_s}\right)\right)$. Let us consider three cases (see Fig. 5): t_{p1}, t_{p2} and t_{p3}, which are all longer than the diffuse double layer charging time τ_{DL}.

The first time t_{p1} is chosen just after the diffuse double layer has been fully charged ($Q_{DL} = C_{DL}V_A/2$), so in good approximation the field in the bulk is approximately zero and a negligible amount of inverse micelles has been adsorbed to the surface. When the voltage over the device is reduced from V_A to $\frac{V_A}{2}$, then the field in the bulk will become $-\frac{V_A}{2d}$ because the voltage drop $\frac{V_A}{2}$ is distributed over the device thickness d. Due to this field, there is a negative current that de-charges the diffuse double layers until a new equilibrium is obtained (the negative current for $t < 1$ s in Fig. 2a). In this new equilibrium the diffuse double layers will contain half of the charge as before, namely $Q_{DL} = C_{DL}V_A/4$, since the voltage across the diffuse double layer capacitance is reduced by a factor 2, and the bulk field will be approximately zero. Since the charging of the Stern layer is proportional to Q_{DL} the Stern layer charging current is expected to be positive, with half the amplitude compared to the case with an applied voltage V_A, precisely as observed in Fig. 2b (blue curve corresponding to $t_p = 1$ s). The exponential decay of the Stern layer charging current is expected to occur with the same time constant τ_s since τ_s is independent of the voltage over the diffuse double layer (see Eq. (20)), as is observed in Fig. 2b.

t_{p2} is chosen at the moment that a charge $\pi_s = C_s\frac{V_A}{4}$ has been accumulated in the Stern layer such that the voltage drop over the Stern layer at both sides has become $\frac{V_A}{4}$ (see Fig. 5b (middle)). After the applied voltage is reduced to $V_A/2$, again a negative current de-charges the diffuse double layers while the Stern layer charge remains approximately the same in this timescale. But after this phase, the voltage over the diffuse double layers and over the bulk has become zero, because the full applied voltage $V_A/2$ is already lost over the two Stern layers. As a result, there is no further Stern layer charging, and no Stern layer charging current, as can be seen in Fig. 2b (green curve for $t_p = 40$ s).

Finally, t_{p3} is taken sufficiently long that the voltage drop over both Stern layers is equal to the applied voltage V_A and the diffuse double layers have disappeared. After reducing the voltage to $V_A/2$, a negative electric field emerges in the bulk and the corresponding negative current builds up a negatively charged diffuse double layer at the optically probed side (grounded) and a positive diffuse double layer at the opposite side, which are therefore oppositely charged as in the polarizing phase. The reduction of the potential difference shown in Fig. 5b, right (red) is directly related to this oppositely charged diffuse double layer. After the bulk field becomes zero and this diffuse double layer is fully established (roughly at $t = t_{p3} + \tau_{DL}$), the adsorption mechanism will now slowly reduce the net charge in the Stern layer, because the diffuse double layers have the opposite charge of the neighboring Stern layers. Therefore, a current with the same amplitude but opposite sign as for the case of t_{p1} is expected. The time-scale of the Stern layer charging is again equal to τ_s.

Since the electrical circuits of the 'Stern layer adsorption' limit (Eqs. (16)–(20)) and the 'adsorption/desorption' limit proposed by Yezer et al. are mathematically equivalent, both models explain the electrical measurements of Span 80 in dodecane [9] or fluorosurfactant in fluorocarbon solvent (this work) equally well. However, the physical interpretation of both models is quite different. The 'adsorption/desorption' limit model [9] is based on a balance between adsorption and desorption of charged inverse micelles at the electrodes, in which the amount of charges in the Stern layer is sufficiently small so there is no associated voltage drop, which is mathematically simplified by taking the adsorption infinitely close to the electrodes. Therefore, after the diffuse double layers are formed in the polarizing step (after τ_{DL}), the diffuse double layers and the voltage drop over the diffuse double layers do not change (visualized in Fig. 5c). So, while in the 'Stern layer adsorption' limit the diffuse double layers gradually disappear over time due to Stern layer charging, in the 'adsorption/desorption' limit the diffuse double layers remain fixed. The exponential decay in the external current originates from the fact that the adsorption flux remains constant while the desorption flux, which is proportional to the accumulated surface charge, increases until it becomes equal to the adsorption flux. After reducing the applied voltage by a factor two, a negative current de-charges the diffuse double layers until the voltage drop over the diffuse double layers (and the associated adsorption flux) reduces by a factor two, independent of the polarizing time. However, the desorption process is proportional to the total charge that has been accumulated during the polarizing voltage step and increases with the time t_p. For example, for t_{p1} the interface charge is still approximately zero, so the interface will keep charging up, but with a current amplitude half the one expected for V_A. For t_{p2} the interface charge already has the equilibrium value corresponding to the applied voltage $V_A/2$, so there is no further electrode charging current. And for t_{p3}, the interface charge is twice the equilibrium value, so the desorption of this excess

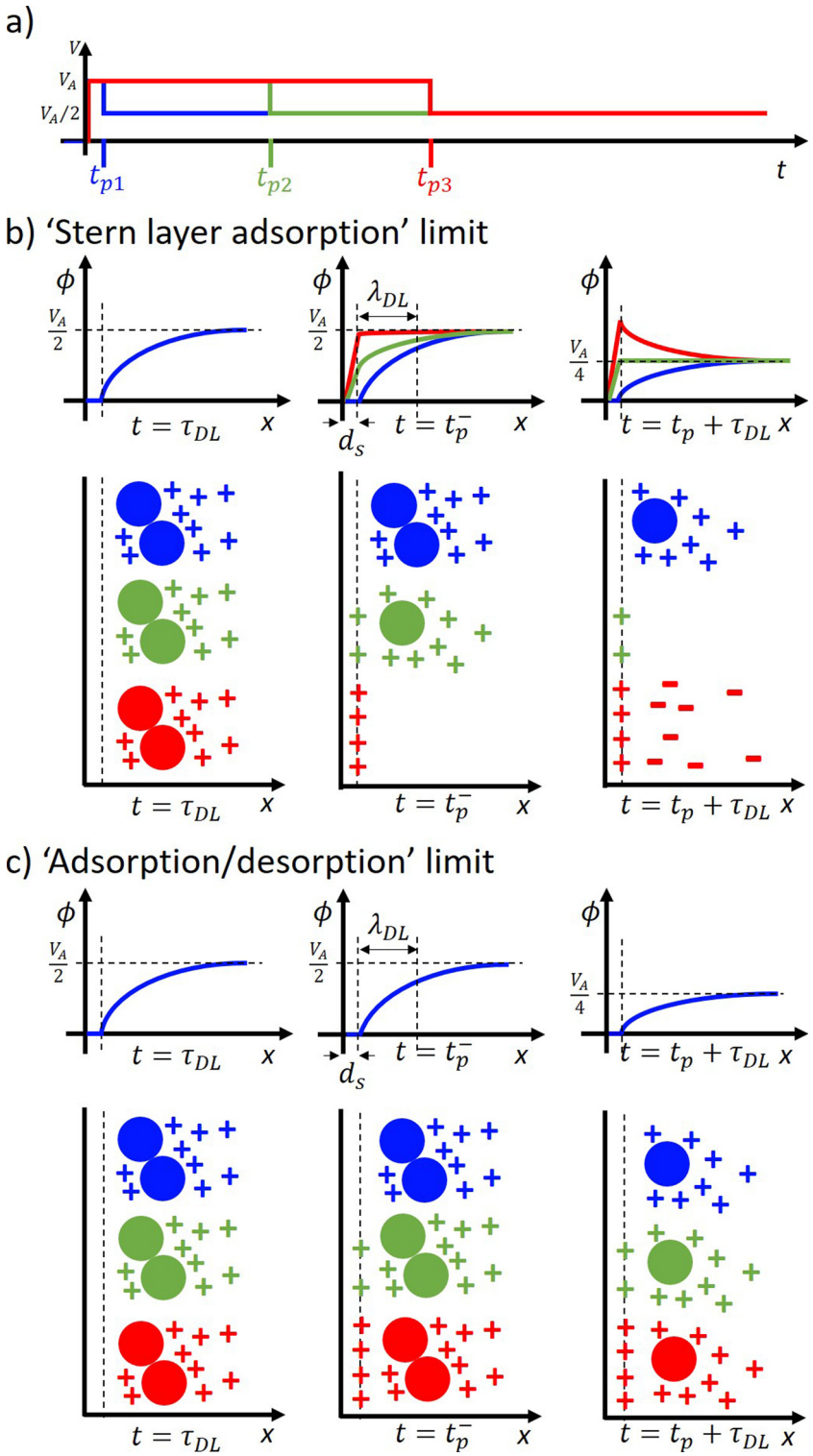

Fig. 5. a) Sketch of the driving voltage sequence, b) Sketch of the potential $\phi(x)$ (top row) and Stern layer charge and diffuse double layer charge (bottom row) for the 'Stern layer adsorption' limit, c) Sketch of the potential $\phi(x)$ (top row) and Stern layer charge and diffuse double layer charge (bottom row) for the 'adsorption/desorption' limit. b) & c) show the situation just after the diffuse double layer formation (left), just before reducing the voltage (middle) and just after the diffuse double layer is formed after reducing the voltage (right). This is visualized for polarizing times t_p much larger than the diffuse double layer time constant τ_{DL} but smaller, similar and larger than the time constant τ_s visualized in blue, green and red, respectively.

will result in a negative current. With this we can now understand why the 'adsorption/desorption' limit leads to the same external electrical currents as predicted by the 'Stern layer adsorption' limit, but with important differences in terms of the presence of diffuse double layers and their associated electrical fields.

Now we analyze the reflectivity measurements given in Fig. 3, in which positively charged colloidal particles are used as an optical probe for determining the electric field in the neighborhood of the electrode where TIR takes place. Using a similar optical configuration as showed in previous work [1], a region of about 100 nm is optically probed,

matching roughly with the diffuse double layer thickness. Following the procedure of [1] the application of a voltage leads to a diffuse double layer of positively charged inverse micelles and pigment particles at the negative electrode, and a diffuse double layer of negatively charged inverse micelles at the positive electrode, shortly after a polarizing voltage is applied. The optical detection of an increased concentration of pigment particles (through a reduced reflectivity) indicates that there is an electric field in the diffuse double layer pointing towards the electrode.

In Fig. 3, the reflectivity for the polarizing voltage step (red) decreases for $t < 10\,\mathrm{s}$ due to the buildup of the diffuse double layer which results in an increase in pigment particles in the optically probed region. For $t > 100\,\mathrm{s}$ the reflectivity increases again, indicating that the concentration of particles in the diffuse double layer decreases. This can be understood if the voltage drop over the diffuse double layer and the corresponding electric field decreases. The behavior and the time dependency of the optical signal are consistent with the predicted reduction of the diffuse double layer charge within the 'Stern layer adsorption' limit derived in Eq. (13), with a time constant of $\tau_s = 450\,\mathrm{s}$. The increase in reflectivity for $t > 100\,\mathrm{s}$ is not explained by the 'adsorption/desorption' limit because in this limit the diffuse double layer charge remains constant after the diffuse double layer formation ($t > 10\,\mathrm{s}$) as derived in Eq. (13). If the diffuse double layer charge remains fixed, the associated field also persists and the pigment particles would stay in the optically probed region, leading to a persisting low reflectivity.

The measurement of the reflectivity (at the electrically grounded side) during the relaxation step ($-0.2\,\mathrm{V}$ to $0\,\mathrm{V}$) after a long negative polarizing step ($t_p \gg \tau_s$) (green curve in Fig. 3c) is also not explained by the 'adsorption/desorption' limit. This behavior is remarkably similar to that for the polarizing voltage step ($0\,\mathrm{V}$ to $+\,0.2\,\mathrm{V}$). This observation is compatible with the Stern layer charging model and can be explained as follows. After a (very) long polarizing voltage step, the applied voltage ($-\,0.2\,\mathrm{V}$) is taken up completely by the Stern layer. By switching the applied voltage to zero, the effective voltage over the bulk becomes equal to $0.2\,\mathrm{V}$, because the voltage over the Stern layers is equal to $-\,0.2\,\mathrm{V}$. The time dependency of the field in the bulk and in the diffuse double layers is then equivalent to the case of a positive polarizing voltage pulse. In the 'adsorption/desorption' limit we expect to have at the probed surface a negatively charged diffuse double layer during the total polarizing step of $-\,0.2\,\mathrm{V}$ (see Eq. (13)). Within the diffuse double layer time $t < \tau_{DL}$ after the relaxation step, this negatively charged diffuse double layer will quickly vanish such that the bulk field becomes zero, since this limiting case assumes there is a negligible voltage drop over the surface charge. Of course, there still is a long-term de-charging current due to the desorption of the negative charges which have been accumulated at the surface. Measurements of reflectivity are in this limit expected to always show a high reflectivity, since no positively charged diffuse double layer (and thus no field and no associated positively charged pigment particles) is formed at the probed surface, neither during the negative polarizing step (when a negatively charged diffuse double layer is present) nor during the relaxation step (since there is no diffuse double layer present).

A third argument supporting the 'Stern layer adsorption' limit is the estimated distance d_s between the charges and the electrode, based on the value of the capacitance per unit area $C_s = \frac{\varepsilon\varepsilon_0}{d_s}$. We find, by fitting C_s from the measured current using Eq. (20), a distance of 1.6 nm for the measurements of Fig. 2 and 0.24 nm for the measurements of Fig. 3. This means that, based on Eqs. (8) and (12), the Stern layer distance d_s should be considerably smaller than 1.6 nm to fit the measurements by a non-negligible desorption. Since we expect d_s to be a few nanometers if the adsorbed inverse micelles stay intact and close to 1 nm if the adsorbed inverse micelle would wet on the surface, d_s is close to its lower limit supporting the 'Stern layer adsorption' limit. For comparison, also in other surfactant systems the adsorption of inverse micelles at the interface has been found to result in similar distances and capacitance values. For example, a 1 nm thickness of the Stern layer for the surfactant AOT in dodecane is calculated by Karvar et al. [14]. For the surfactant Span 80 in dodecane and Span 20 in dodecane the capacitance per unit area $C_{ads} = \frac{k_a \tau_d \varepsilon\varepsilon_0}{\lambda_{DL}^2}$ introduced by Yezer et al. (Eq. 23 in [9]) has been interpreted within the 'adsorption/desorption' limit [9]. We will here reinterpret these capacitance values within the 'Stern layer adsorption' limit to find the maximal Stern layer distance allowed for the general model (Eq. (12)). Based on the measurements provided in [9], we obtain: for 3 mM Span 80 in dodecane $d_s = 0.6\,\mathrm{nm}$ (estimated values: $k_a = 5\frac{\mu\mathrm{m}}{\mathrm{s}}$, $\lambda_{DL} = 0.55\,\mu\mathrm{m}$ and $\tau_d = 100\,\mathrm{s}$), for 90 mM Span 80 in dodecane $d_s = 0.3\,\mathrm{nm}$ (estimated values: $k_a = 5\frac{\mu\mathrm{m}}{\mathrm{s}}$, $\lambda_{DL} = 0.08\,\mu\mathrm{m}$ and $\tau_d = 5\,\mathrm{s}$) and for 10 mM Span 20 in dodecane $d_s = 0.7\,\mathrm{nm}$ (estimated values: $k_a = 10\frac{\mu\mathrm{m}}{\mathrm{s}}$, $\lambda_{DL} = 0.1\,\mu\mathrm{m}$ and $\tau_d = 1.5\,\mathrm{s}$). These nonpolar systems all give Stern layer distances in the nanometer range even though they use different surfactants, concentrations and solvents. The obtained maximum for d_s appears to be physically close to a minimal value for d_s that results in a non-negligible voltage drop over the Stern layer and, based on Eq. (8), a much longer desorption time constant than found within the 'adsorption/desorption' limit. All calculated values for d_s are close to (or slightly smaller than) the expected inverse micelle radius. The obtained values for the Stern layer distance may be an underestimation because we used the dielectric constant of the solvent, which is probably somewhat smaller than the equivalent value for inverse micelles. Also surface roughness may lead to an underestimation of the Stern layer distance. Overall, we arrive at an estimated physical thickness of the Stern layer on the order of 1 nm.

And fourthly, based on Eq. (8) we see that the only relation between τ_{eff} and the surfactant concentration is through λ_{DL} which is proportional with $\frac{1}{\sqrt{\bar{n}}}$. We find that τ_{eff} is independent of the concentration within the 'adsorption/desorption' limit while it is inversely proportional to the concentration within the 'Stern layer adsorption' limit. As has been noted by Yezer et al. [9] (visualized in Fig. 16 in [9]), the measured time constants requires that the desorption rate should be proportional not only with the adsorbed surface charge concentration but also with the concentration of surfactant. Interpreted in the general model, this means that the measured τ_{eff} is inversely proportional with $\bar{n}$ which is the case for the 'Stern layer adsorption' limit. In order to fit to the 'adsorption/desorption' limit one needs to alter the theory of the desorption mechanism and possible explanations are therefore more complex, for example desorption also involving interactions with uncharged inverse micelles.

A side note must be made for the 'Stern layer adsorption' limit. Since this limit only considers the adsorption of charged inverse micelles, the surface will be collecting charges of both polarities over time since we assume that a charged inverse micelle is not able to desorb. To avoid that all surfactant would end up at the surfaces, we can assume that positive and negative inverse micelles at the same surface can recombine into neutral micelles (comproportionation) which then desorb from the surface.

Even though different surfactant systems are used in our work (fluorosurfactant in fluorocarbon solvents with and without pigment particles) and in the work by Yezer et al. [9] (Span 80 in dodecane and Span 20 in dodecane) the above arguments suggest that the long-term charging for all these experiments originates from the formation of a Stern layer.

6. Conclusion

We have investigated the long-term electro-optical behavior of devices containing a fluorosurfactant in fluorocarbon solvent using electrical and optical measurements. To explain the observed long-term effects, we propose a general model which includes adsorption of charged inverse micelles, charge accumulation within a Stern layer and desorption of charged inverse micelles. We compare two limiting cases of this model, the 'adsorption/desorption' limit and the 'Stern layer

adsorption' limit. An important difference between both limits is that in the 'Stern layer adsorption' limit the voltage drop over the diffuse double layer vanishes during a long polarizing step, while in the 'adsorption/desorption' limit the diffuse double layer remains constant during the polarizing step. Transient current measurements and optical measurements, where we visualize the electric field in the diffuse double layer by means of added positively charged pigment particles, are conducted. Both limits of the general model can equally explain the electrical current measurements, and the 'Stern layer adsorption' limit additionally explains the optical measurements for polarizing voltages as well as for relaxation voltages. The 'Stern layer adsorption' limit assumes that charges from the diffuse double layer are adsorbed over long time-scales in a Stern layer with a thickness on the order of the inverse micelle size. This model fits our data in fluorocarbon solvents as well as previously reported data by Karvar et al. for AOT in dodecane [14] and the measurements over a range of concentrations of Span 80 and Span 20 in dodecane reported by Yezer et al. [9].

CRediT authorship contribution statement

Bavo Robben: Data curation, Formal analysis, Investigation, Methodology, Software, Validation, Visualization, Writing - original draft. **Filip Beunis:** Writing - review & editing. **Kristiaan Neyts:** Project administration, Writing - review & editing. **Michiel Callens:** Investigation, Writing - review & editing. **Thomas Johansson:** Investigation, Writing - review & editing. **Graham Beales:** Investigation, Writing - review & editing. **Robert Fleming:** Project administration, Resources, Writing - review & editing. **Filip Strubbe:** Supervision, Writing - review & editing.

Declaration of Competing Interest

The authors declare that they have no known competing financial interests or personal relationships that could have appeared to influence the work reported in this paper.

Acknowledgments

The authors would like to acknowledge Merck KGaA for providing the chemical components and the Research Foundation-Flanders (FWO) for funding through the Strategic Basic Research grant 1S67017N.

References

[1] B. Robben, F. Beunis, K. Neyts, R. Fleming, B. Sadlik, T. Johansson, L. Whitehead, F. Strubbe, Electrodynamics of electronic paper based on total internal reflection, Phys. Rev. Appl. 10 (34041) (2018).
[2] F. Strubbe, F. Beunis, T. Brans, M. Karvar, W. Woestenborghs, K. Neyts, Electrophoretic retardation of colloidal particles in nonpolar liquids, Phys. Rev. X 3 (021001) (2013).
[3] T. Sugita, T. Ohshima, Evaluation of electrophoretic migration of submicron particles in a microgap by optical and current responses, J. Appl. Phys. 49 (2010).
[4] T. Sugita, T. Ohshima, Evaluation of electrophoretic migration by optical and current responses to cyclic-polarity-reversed triangular voltage, J. Appl. Phys. 50 (2011).
[5] F. Strubbe, F. Beunis, M. Marescaux, B. Verboven, K. Neyts, Electrokinetics of colloidal particles in nonpolar media containing charged inverse micelles, Appl. Phys. Lett. 93 (11) (2008).
[6] F. Strubbe, K. Neyts, Charge transport by inverse micelles in non-polar media, J. Phys. Condens. Matter 29 (453003) (2017).
[7] F. Beunis, F. Strubbe, M. Karvar, O. Drobchak, T. Brans, K. Neyts, Inverse micelles as charge carriers in nonpolar liquids: characterization with current measurements, Curr. Opin. Colloid Interface Sci. 18 (129) (2013).
[8] B.A. Yezer, A.S. Khair, P.J. Sides, D.C. Prieve, Journal of Colloid and Interface Science Use of electrochemical impedance spectroscopy to determine double-layer capacitance in doped nonpolar liquids, J. Colloid Interface Sci. 449 (2) (2015).
[9] B.A. Yezer, A.S. Khair, P.J. Sides, D.C. Prieve, Determination of charge carrier concentration in doped nonpolar liquids by impedance spectroscopy in the presence of charge adsorption, J. Colloid Interface Sci. 469 (325) (2016).
[10] J. Lee, Z.L. Zhou, G. Alas, S.H. Behrens, Mechanisms of particle charging by surfactants in nonpolar dispersions, Langmuir 31 (11989) (2015).
[11] F. Strubbe, M. Prasad, F. Beunis, Characterizing generated charged inverse micelles with transient current measurements, J. Phys. Chem. A 119 (1957) (2015).
[12] F. Beunis, F. Strubbe, M. Marescaux, J. Beeckman, K. Neyts, A.R.M. Verschueren, Dynamics of charge transport in planar devices, Phys. Rev. E 78 (011502) (2008).
[13] F. Beunis, F. Strubbe, M. Marescaux, K. Neyts, A.R.M. Verschueren, Diffuse double layer charging in nonpolar liquids, Appl. Phys. Lett. 91 (2007).
[14] M. Karvar, F. Strubbe, F. Beunis, R. Kemp, A. Smith, M. Goulding, K. Neyts, Transport of charged Aerosol OT inverse micelles in nonpolar liquids, Langmuir 27 (10386) (2011).
[15] J. Lee, Z. Zhou, S.H. Behrens, Interfaces charged by a nonionic surfactant, research-article, J. Phys. Chem. B 122 (6101) (2018).
[16] E.L. Michor, B.S. Ponto, J.C. Berg, Effects of Reverse Micellar Structure on the Particle Charging Capabilities of the Span Surfactant Series, (2016).
[17] E.L. Michor, J.C. Berg, The particle charging behavior of ion-exchanged surfactants in apolar media, Colloids Surf. A Physicochem. Eng. Asp. 512 (1) (2017).
[18] G.N. Smith, J. Eastoe, Controlling colloid charge in nonpolar liquids with surfactants, J. Chem. Soc. Faraday Trans. 424 (2013).
[19] J.R. Macdonald, Impedance spectroscopy, Ann. Biomed. Eng. 20 (289) (1992).
[20] F. Strubbe, A.R.M. Verschueren, L.J.M. Schlangen, F. Beunis, K. Neyts, Generation current of charged micelles in nonaqueous liquids: measurements and simulations, J. Colloid Interface Sci. 300 (396) (2006).